Multiple photodetachment of oxygen anions via *K*-shell excitation and ionization: Direct double-detachment processes and subsequent deexcitation cascades

S. Schippers,[1,*] A. Hamann,[1] A. Perry-Sassmannshausen,[1] T. Buhr,[1] A. Müller,[1] M. Martins,[2] S. Reinwardt,[2] F. Trinter,[3,4] and S. Fritzsche[5,6,7]

[1]*I. Physikalisches Institut, Justus-Liebig-Universität Gießen, Heinrich-Buff-Ring 16, 35392 Giessen, Germany*
[2]*Institut für Experimentalphysik, Universität Hamburg, Luruper Chaussee 149, 22761 Hamburg, Germany*
[3]*Institut für Kernphysik, Goethe-Universität Frankfurt am Main, Max-von-Laue-Straße 1, 60438 Frankfurt am Main, Germany*
[4]*Molecular Physics, Fritz-Haber-Institut der Max-Planck-Gesellschaft, Faradayweg 4-6, 14195 Berlin, Germany*
[5]*Helmholtz-Institut Jena, Fröbelstieg 3, 07743 Jena, Germany*
[6]*Theoretisch-Physikalisches Institut, Friedrich-Schiller-Universität Jena, Max-Wien-Platz 1, 07743 Jena, Germany*
[7]*GSI Helmholtzzentrum für Schwerionenforschung, Planckstraße 1, 64291 Darmstadt, Germany*

(Received 7 June 2022; accepted 14 July 2022; published 28 July 2022)

Experimental cross sections for m-fold photodetachment ($m = 2$–5) of oxygen anions via K-shell excitation and ionization were measured in the photon-energy range of 525–1500 eV using the photon-ion merged-beams technique at a synchrotron light source. The measured cross sections exhibit clear signatures of direct double detachment, including double K-hole creation. The shapes of the double-detachment cross sections as a function of photon energy are in accord with Pattard's [J. Phys. B **35**, L207 (2002)] empirical scaling law. We have also followed the complex de-excitation cascades that evolve subsequently to the initial double-detachment events by systematic large-scale cascade calculations. The resulting theoretical product charge-state distributions are in good agreement with the experimental findings.

DOI: 10.1103/PhysRevA.106.013114

I. INTRODUCTION

Atomic anions are peculiar quantum systems since their extra electron is (weakly) bound by short-range forces, resulting from the induced polarization of the atomic electron shells [1–3]. In the O^- ($1s^2\,2s^2\,2p^5\;{}^2P_{3/2}$) ground level, the binding energy of the most loosely bound electron is only 1.461 eV [4], while the ionization energy of neutral oxygen atoms amounts to 13.681 eV [5]. A fundamental process that allows one to probe electron-electron correlation effects in atomic anions is single photodetachment (SD), i.e., the removal of an electron by absorption of a single photon. Recent studies on multiple photodetachment of F^- [6] and C^- [7] have somewhat unexpectedly revealed that atomic anions are also ideal systems for studying direct double detachment (DD), where one photon simultaneously ejects two electrons (see also Ref. [8]). For F^-, the cross section for simultaneous ejection of a $1s$ and a $2p$ electron could be extracted from the measured data for photon energies that range from below the threshold for direct double detachment of a $1s$ and a $2p$ electron ($1s$+$2p$ DD) to well beyond the cross-section maximum. This result has already stimulated a successful effort to theoretically describe the cross section for this many-particle effect with two electrons ending up in the continuum [9]. For C^-, the cross section for double-core hole formation by a single photon ($1s$+$1s$ DD) was measured. Surprisingly, this cross section was about an order of magnitude larger than what was expected on the basis of previous results on the double core-hole creation in carbon-containing molecules [10].

In order to shed more light on the role of DD processes in the inner-shell photodetachment of atomic anions, the present study extends the above-mentioned previous work to the O^- anion. Double detachment, or double ionization for neutral atoms and positive ions, has been repeatedly studied in the literature, mostly for helium-like systems. Since a historical account has already been given in Ref. [6], we shall mention here only the work that is most closely related to the present investigation, i.e., studies on DD of H^- [11], He^- [12], and K^- [13], where the corresponding cross sections were scanned over very narrow photon-energy ranges of a few meV in the vicinity of the respective thresholds. Earlier studies on net double and triple inner-shell detachment of O^- ions also considered only quite limited photon-energy ranges and focused on the $1s\,2s^2\,2p^6$ resonance at 525.6 eV that is associated with $1s \rightarrow 2p$ photoexcitation [14,15].

When compared with the previous measurements, the present photon-energy range of 525–1500 eV is much wider and comprises the thresholds for direct single detachment of a $1s$ electron ($1s$ SD) at 529.6 eV [15] as well as the thresholds for $1s$+$2p$ DD, $1s$+$2s$ DD, and $1s$+$1s$ DD. The threshold for the latter process occurs at about 1100 eV (see below). Our experimental cross sections σ_m for m-fold photodetachment of O^- ions with $m = 2, 3, 4, 5$ exhibit signatures of all these processes. m-fold photoionization results in the production of multiply positively charged $O^{(m-1)+}$ ions and can be

*stefan.schippers@physik.uni-giessen.de

represented as

$$h\nu + \mathrm{O}^- \rightarrow \mathrm{O}^{(m-1)+} + m\,e^-. \quad (1)$$

In addition to experimental cross sections for the production of $\mathrm{O}^{(m-1)+}$ ions, we present theoretical results for O^- photoabsorption. Using a recently developed theoretical toolbox [16,17], we model the complex de-excitation cascades that follow the creation of single or double inner-shell holes and thus give rise to photon-energy-dependent distributions of product-ion charge states.

II. EXPERIMENT

The measurements were carried out using the photon-ion merged-beams technique [18] at the PIPE facility [19–21], which is a permanently installed end station at the photon beamline P04 [22] of the synchrotron radiation source PETRA III operated by Deutsches Elektronensynchrotron (DESY) in Hamburg, Germany. Oxygen anions were produced by a Cs-sputter ion source [23] with a sputter target made of solid aluminum oxide and a sputter potential of about 2 kV. After acceleration to a kinetic energy of 6 keV, the ions were passed through an analyzing dipole magnet which was adjusted such that $^{16}\mathrm{O}^-$ ions were selected for further transport to the photon-ion merged-beams interaction region. The ion current in the interaction region was up to 350 nA (18 nA) with the ion beam being uncollimated (collimated to about 2×2 mm^2). These values are an order of magnitude larger than what could be achieved in our previous study where a different type of ion source was used [15].

In the interaction region, where the residual-gas pressure was in the mid-10^{-10} mbar range, the ion beam was coaxially merged with the counterpropagating soft x-ray photon beam over a distance of about 1.7 m. $\mathrm{O}^{(m-1)+}$ ions as obtained from multiple photodetachment [Eq. (1)] were separated from the primary ion beam by a second dipole magnet. Inside this magnet, a Faraday cup collected the primary ion beam, while the charge-selected product ions were directed to the detector chamber. Along their flight path, they first passed through a spherical 180-deg out-of-plane deflector to suppress background from stray electrons, photons, and ions before the ions then entered a single-particle detector with nearly 100% detection efficiency [24].

The dark-count rate of our detector amounted to ≈ 0.02 Hz (see also Ref. [25]). In each product-ion channel, this contributed to a photon-energy-independent background count rate. Other contributions to the background count rate arose from collisions of the primary ions with residual-gas particles, where electrons can be lost from the projectiles by stripping reactions. This contribution to the energy-independent background was particularly noticeable in the double-detachment channel, but practically negligible for triple, fourfold, and fivefold detachment. For double detachment, the background was determined by recording O^+ product ions while alternatingly switching the photon beam on and off by opening and closing a fast beam shutter in the photon beamline.

Relative cross sections for m-fold photodetachment were obtained by normalizing the background-subtracted count rates of $\mathrm{O}^{(m-1)+}$ product ions on the primary O^- ion current and on the photon flux measured with a calibrated photodiode. The energy-dependent photon flux reached its peak of 3×10^{13} s^{-1} at photon energies around 850 eV and at a photon-energy spread of ≈ 1 eV. This spread also depended on the photon energy ranging from ≈ 0.4 eV at 500 eV up to ≈ 2.5 eV at 1500 eV for a nominal width of the monochromator exit slit of 1000 μm. The relative cross sections were put on an absolute scale by using our previously measured absolute cross sections for single and double detachment of O^- as reference values [15]. The systematic uncertainty of the experimental absolute cross sections is estimated to be $\pm 15\%$ at 90% confidence level [19].

The photon-energy scale was calibrated by absorption measurements in nitrogen gas using the lowest vibrational component of the $1s \rightarrow \pi^*$ resonance at 400.86(3) eV (see discussion by Müller *et al.* [26] and references therein) as a calibration point. A second (intrinsic) calibration point was provided by the $\mathrm{O}^-(1s \rightarrow 2p)$ resonance at 525.6(1) eV [15]. In addition, the Doppler shift that is associated with the ion-beam velocity was taken into account. It amounted to 0.467 eV at 520 eV and to 1.346 eV at 1500 eV. The remaining uncertainty of the calibrated photon-energy scale is estimated to be ± 0.2 eV for photon energies of less than 600 eV. Since there are no calibration points at higher energies, the uncertainty increases with increasing photon energy. At a photon energy of 1500 eV, it is estimated to amount to about ± 2 eV.

III. COMPUTATIONS

Extended energy-level and transition-rate calculations need to be performed to model the successive (photo-)detachment from negative ions. For inner-shell-excited atoms and ions, the multiconfiguration Dirac-Hartree-Fock (MCDHF) method [27,28] has been found to be a versatile tool to model the—radiative and nonradiative—decay and to describe the interplay of different atomic processes in course of their relaxation. In this work, all calculations have been performed by means of the JAC toolbox, the Jena atomic calculator [16], which has been expanded recently to follow rather long ionization pathways. Not much needs to be said about how such cascade computations are implemented in practice [17,29], and we just summarize a few major steps that have been carried out. The numerical results of these simulations will then be discussed together with the measurements below.

The photoexcitation and ionization of an electron requires first of all insight into the $1s^{-1}$ and $(1s\,n\ell)^{-2}$ threshold energies and the associated cross sections. This refers to both the excitation and decay of the core-excited $1s\,2s^2\,2p^6\;{}^2S_{1/2}$ level of the O^- ion and the core-detached O^-, that is, $1s\,2s^2\,2p^5\;{}^{1,3}P_J$ core-excited levels of the neutral atom, as well as of various doubly core-excited configurations. In particular, the $1s\,2s^2\,2p^4\,3p$, $1s\,2s^2\,2p^4$, and $1s\,2s\,2p^5$ configurations play a prominent role in the cascade decay of $1s$ core-detached neutral oxygen and have been included in the computations. The probabilities for different shake transitions have been determined from the orbital overlap of the $1s^2\,2s^2\,2p^5$ ground configuration and the $1s2s^22p^5 + 1s\,2s^2\,2p^4\,(3p + 4p)$ configurations, and show that up to 10% of the $2p$ electrons are *shaken* to orbitals with higher n or even into the continuum. A similar shake probability is expected for the $2s$ electrons, although their contributions to the photodetachment cross sec-

TABLE I. Computed threshold energies for single detachment (SD) and double detachment (DD) of O^-. The energy ranges comprise all fine-structure levels that belong to the specified configurations.

Configuration	Process	Energy (eV)
$1s^1\,2s^2\,2p^5$	$1s$ SD	529.8–532.5
$1s^1\,2s^2\,2p^4$	$1s$+$2p$ DD	545.2–553.8
$1s^1\,2s^1\,2p^5$	$1s$+$2s$ DD	561.9–574.0
$2s^2\,2p^5$	$1s+1s$ DD	1160.2

tions are more difficult to assess. Below, we make use of these shake probabilities for estimating the ion distributions at photon energies $\hbar\omega \gtrsim 450$ eV.

Apart from the excitation energies and absorption strengths for creating a $1s$ inner-shell hole, the main computational focus was placed upon the stepwise relaxation and, hence, the (relative) ion distributions that can be directly compared with the experiment. This stepwise relaxation can be formally described by an *atomic cascade* that connects ions of different charge states to each other via different (decay) processes. This relaxation proceeds until a given number of electrons is released and/or the ions cannot further decay to any lower level. Such cascades therefore require us to automatically determine all single configurations that may energetically occur due to various photoemission and autoionization processes from the initially chosen hole configurations and levels, and to include a proper number of shake configurations. To support a detailed analysis of different models, we therefore distinguish in JAC between (so-called) cascade *computations* and *simulations*; cf. Ref. [17].

In practice, any computation starts from setting up a cascade *tree*, i.e., the list of configurations (Tables II) and associated levels that likely contribute to the relaxation of the ions. These levels are then divided into (blocks of) multiplets from which the various decay pathways can be readily derived. A pathway hereby refers to a sequence of two or more

TABLE II. Simplified scheme of the cascade that sets in subsequent to $1s$ SD of $O^-(1s^2\,2s^2\,2p^5)$. The scheme contains all energetically allowed single-step autoionizing transitions and dipole-allowed radiative transitions. Right arrows and down-right arrows denote Auger transitions from the configuration to the left and radiative transitions from a configuration above, respectively. The ground configurations of the different product ions, which are usually reached via multiple pathways, are printed in boldface.

O	O^+	O^{2+}
$1s^1\,2s^2\,2p^5$	$\rightarrow$ **$1s^2\,2s^2\,2p^3$**	
	$\rightarrow 1s^2\,2s^1\,2p^4$	$\rightarrow$ **$1s^2\,2s^2\,2p^2$**
	$\downarrow$ **$1s^2\,2s^2\,2p^3$**	
	$\rightarrow 1s^2\,2s^0\,2p^5$	$\rightarrow 1s^2\,2s^1\,2p^3$
		$\downarrow$ **$1s^2\,2s^2\,2p^2$**
	$\downarrow 1s^2\,2s^1\,2p^4$	$\rightarrow$ **$1s^2\,2s^2\,2p^2$**
	$\downarrow$ **$1s^2\,2s^2\,2p^4$**	
$\downarrow 1s^2\,2s^2\,2p^4$		
$\downarrow 1s^2\,2s^1\,2p^5$	$\rightarrow$ **$1s^2\,2s^2\,2p^3$**	
$\downarrow$ **$1s^2\,2s^2\,2p^4$**		

TABLE III. Simplified scheme of the cascade that sets in subsequent to $1s$+$2p$ DD of $O^-(1s^2\,2s^2\,2p^5)$. The scheme contains all energetically allowed single-step autoionizing transitions and dipole-allowed radiative transitions. See Table II for further details.

O^+	O^{2+}	O^{3+}
$1s^1\,2s^2\,2p^4$	$\rightarrow$ **$1s^2\,2s^2\,2p^2$**	
	$\rightarrow 1s^2\,2s^1\,2p^3$	$\rightarrow$ **$1s^2\,2s^2\,2p^1$**
	$\downarrow$ **$1s^2\,2s^2\,2p^2$**	
	$\rightarrow 1s^2\,2s^0\,2p^4$	$\rightarrow 1s^2\,2s^1\,2p^2$
		$\downarrow$ **$1s^2\,2s^2\,2p^1$**
	$\downarrow 1s^2\,2s^1\,2p^3$	$\rightarrow$ **$1s^2\,2s^2\,2p^1$**
	$\downarrow$ **$1s^2\,2s^2\,2p^2$**	
$\downarrow 1s^2\,2s^2\,2p^3$		
$\downarrow 1s^2\,2s^1\,2p^4$	$\rightarrow$ **$1s^2\,2s^2\,2p^2$**	
$\downarrow$ **$1s^2\,2s^2\,2p^3$**		

levels, which can be subsequently occupied in the course of the relaxation and whose number rapidly increases with (i) the number of open shells involved for an ion and (ii) the depth of the cascade. The major computational effort refers, however, to the *representation* of the fine-structure levels for

TABLE IV. Simplified scheme of the cascade that sets in subsequent to $1s$+$2s$ DD of $O^-(1s^2\,2s^2\,2p^5)$. The scheme contains all energetically allowed single-step autoionizing transitions and dipole-allowed radiative transitions. See Table II for further details. In principle, the $O^{3+}(1s^2\,2s^1\,2p^2) \rightarrow O^{4+}(1s^2\,2s^2)$ and $O^{3+}(1s^2\,2s^0\,2p^3) \rightarrow O^{4+}(1s^2\,2s\,2p)$ transitions could be conceived, but these are energetically not possible.

O^+	O^{2+}	O^{3+}
$1s^1\,2s^1\,2p^5$	$\rightarrow 1s^1\,2s^2\,2p^3$	$\rightarrow$ **$1s^2\,2s^2\,2p^1$**
		$\rightarrow 1s^2\,2s^1\,2p^2$
		$\downarrow$ **$1s^2\,2s^2\,2p^1$**
		$\rightarrow 1s^2\,2s^0\,2p^3$
		$\downarrow 1s^2\,2s^1\,2p^2$
		$\downarrow$ **$1s^2\,2s^2\,2p^1$**
	$\downarrow$ **$1s^2\,2s^2\,2p^2$**	
	$\rightarrow 1s^2\,2s^1\,2p^3$	$\rightarrow$ **$1s^2\,2s^2\,2p^1$**
	$\downarrow$ **$1s^2\,2s^2\,2p^2$**	
	$\rightarrow 1s^2\,2s^0\,2p^4$	$\rightarrow 1s^2\,2s^1\,2p^2$
		$\downarrow$ **$1s^2\,2s^2\,2p^1$**
	$\downarrow 1s^2\,2s^1\,2p^3$	$\rightarrow$ **$1s^2\,2s^2\,2p^1$**
	$\downarrow$ **$1s^2\,2s^2\,2p^2$**	
$\downarrow 1s^1\,2s^2\,2p^4$	$\rightarrow$ **$1s^2\,2s^2\,2p^2$**	
	$\rightarrow 1s^2\,2s^1\,2p^3$	
	$\downarrow$ **$1s^2\,2s^2\,2p^2$**	
	$\rightarrow 1s^2\,2s^0\,2p^4$	$\rightarrow 1s^2\,2s^1\,2p^2$
		$\downarrow$ **$1s^2\,2s^2\,2p^1$**
	$\downarrow 1s^2\,2s^1\,2p^3$	$\rightarrow$ **$1s^2\,2s^2\,2p^1$**
	$\downarrow$ **$1s^2\,2s^2\,2p^2$**	
$\downarrow 1s^2\,2s^1\,2p^4$	$\rightarrow$ **$1s^2\,2s^2\,2p^2$**	
$\downarrow$ **$1s^2\,2s^2\,2p^3$**		
$\downarrow 1s^2\,2s^0\,2p^5$	$\rightarrow 1s^2\,2s^1\,2p^3$	
	$\downarrow$ **$1s^2\,2s^2\,2p^2$**	
$\downarrow 1s^2\,2s^1\,2p^4$		
$\downarrow$ **$1s^2\,2s^2\,2p^3$**		

each intermediate step (block) of the cascade as well as to the computation of the transition amplitudes.

To establish a hierarchy of useful cascade models, different approaches are distinguished in JAC in order to support and analyze a systematically improved representation of the fine structure and amplitudes. Unlike for Si^- ions [30], the rather simple shell structure of O^- with just a $1s^2\,2s^2\,2p^5$ ground configuration enables us to apply a self-consistent treatment of all blocks of the cascades (approach B), in addition to just an *averaged* single-configuration approach (approach A). Indeed, approach A, as the simplest, neglects all configuration mixing between the bound-state levels and also restricts the computations to just a single set of continuum orbitals for each *step* of the cascade [31]. In contrast, approach B applies an individual self-consistent field and set of orbitals for all blocks of the cascade, while each electron configuration in the decay tree still forms a single multiplet with a well-defined fine structure (configuration mixing) by diagonalizing the Hamiltonian matrix of this configuration. This single-configuration approach is expected to already provide a quite reasonable description of the strongest decay paths. For analyzing the ion distribution below, we calculated the stepwise decay of the three initial configurations $1s\,2s^2\,2p^5$ (Table II), $1s\,2s^2\,2p^4$ (Table III), and $1s\,2s\,2p^5$ (Table IV) and for the release of up to five electrons. These ion distributions are then combined with the shake probabilities to estimate the (relative) m-fold photodetachment cross sections and for comparison with the experiment. The results from these simulations are shown and discussed below in Sec. IV. Despite the improved modeling with approach B, the quite limited representation of the fine-structure levels and the need for including different shake transitions are likely the main reasons for the remaining deviations of the predicted ion distributions from the measurements. In addition to the cascades that follow the creation of one $1s$ hole, we also treated in a similar manner the cascades that result from double core-hole creation. In these calculations, all together 23 configurations with 3–7 electrons and 83 cascade steps were considered, a tabulation of which similar to Tables II–IV would exceed one page.

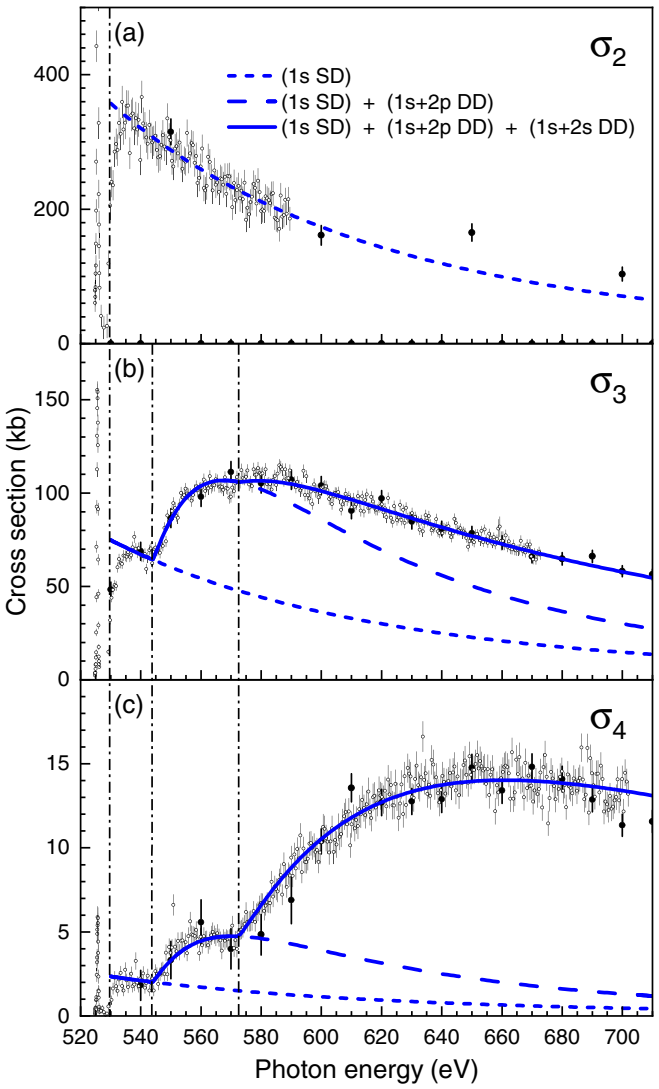

FIG. 1. Experimental cross sections for double (a), triple (b), and quadruple (c) photodetachment of O^- ions. The open symbols represent fine scans over a narrower energy range and the more widely spaced full symbols represent coarse scans that extend to higher energies of up to 1500 eV (see Fig. 3). The vertical dash-dotted lines at 529.6, 543.9, and 572.5 eV mark the thresholds for $1s$ SD, $1s{+}2p$ DD, and $1s{+}2s$ DD respectively. The full lines result from a simultaneous fit of empirical cross section formulas for these three ionization processes to the three experimental fine-scan data sets (see text) with the individual contributions being represented by the dashed lines as explained by the legend in panel (a).

IV. RESULTS AND DISCUSSION

Figure 1 displays the measured cross sections σ_2, σ_3, and σ_4 for double, triple, and fourfold detachment of O^-. The $1s\,2s^2\,2p^6\ ^2S_{1/2}$ resonance at 525.6 eV can be discerned in each of the three cross sections. Its resonance parameters were already determined from our previously measured high-resolution data [15]. We used this previous analysis for determining the experimental photon-energy spread ΔE by fitting a Voigt profile to the resonance. In the fit, the Gaussian full width at half maximum (FWHM), ΔE, was treated as a free parameter. The fit gave rise to a spread of $\Delta E \approx 0.4$ eV.

In our previous work on multiple photodetachment of C^- ions [7], we discovered a number of previously unknown resonances, in particular, for the triple-detachment cross section. Within the limits of the present statistical uncertainties, none of the cross sections displayed in Fig. 1 shows any signs of further resonance features in addition to the $1s\,2s^2\,2p^6\ ^2S_{1/2}$ resonance at 525.6 eV. In the search for additional resonances, we have also performed scans of σ_3 with lower photon-energy spread and higher point density, but these did not result in any further resonances. We therefore conclude that the O^- anion does not feature any strong excitation channels to more highly excited autoionizing levels beyond the $1s\,2s^2\,2p^6\ ^2S_{1/2}$ level.

In our earlier O^- experiment [15], the photon-energy range extended only to a few eV above the threshold for $1s$ SD at 529.6 eV. The new measurements extend to much higher energies where the cross sections σ_3 [Fig. 1(b)] and σ_4 [Fig. 1(c)] exhibit additional thresholds at 543.9 and 572.5 eV. According to our atomic-structure calculations (Table I), these thresholds, which are not discernible in σ_2 [Fig. 1(a)], correspond

to the simultaneous removal of two electrons by one photon, i.e., to direct $1s{+}2p$ DD and $1s{+}2s$ DD, respectively.

The cross section σ_2 for net double detachment does not exhibit any significant DD features, since the Auger processes, that follow the initial double core-hole creation, further increase the charge state of the intermediate O^+ ion (created by DD of O^-) with a probability of almost 100%. Therefore, above the threshold for $1s$ SD at 529.6 eV, the cross section σ_2 is practically exclusively due to this single-detachment process. For the purpose of curve fitting, we have parameterized the cross section for $1s$ SD following a prescription of Verner *et al.* [32]. We have determined the according parameter values by a fit to σ_2[1]. The resulting curve $\sigma_{1s}^{(SD)}(E)$ is displayed as the short-dashed line in Fig. 1(a). Above the threshold, the fit matches the experimental data. The agreement is, however, less convincing at the threshold. This can be attributed to the fact that the Verner formula, which was originally designed for photoionization cross sections of positively charged ions [32], does not account for the more gently rising photodetachment thresholds of negative ions. Nevertheless, the fit provides a realistic extrapolation of the $1s$ SD cross section toward higher energies as required below.

The $1s$ SD process also contributes to the cross sections for net triple and fourfold detachment displayed in Figs. 1(b) and 1(c), respectively. However, above the thresholds for $1s{+}2p$ DD and $1s{+}2s$ DD, these latter processes dominate the cross sections σ_3 and σ_4. The cross section for net fourfold detachment rises from 5 kb at the $1s{+}2s$ DD threshold to a maximum value of 14 kb at about 650 eV. The corresponding rise is barely visible in the cross section for triple detachment, which nevertheless exhibits a strong contribution by $1s{+}2p$ DD leading to a cross-section rise from $\approx$70 kb at the $1s{+}2p$ DD threshold to $\approx$105 kb at the $1s{+}2s$ DD threshold.

As demonstrated earlier [6,7,33], the DD contributions to the measured cross sections can be represented as functions of the photon energy E by a semiempirical formula, that has been devised by Pattard [34]:

$$\sigma^{(DD)}(E) = \sigma^{(\max)} x^{\alpha} \left(\frac{\alpha + 7/2}{x\alpha + 7/2} \right)^{\alpha+7/2}, \qquad (2)$$

where $x = (E - E^{(\mathrm{th})})/(E^{(\max)} - E^{(\mathrm{th})})$, $E^{(\mathrm{th})}$ is the threshold energy and $\alpha = 1.1269$ is the Wannier exponent. Its numerical value [35] is the appropriate one for the charge of the doubly detached intermediate O^+ ion, which results from direct double detachment of O^-. Furthermore, in Eq. (2), $\sigma^{(\max)}$ is the cross-section maximum, which occurs at the energy $E^{(\max)}$. Numerical values for these parameters were obtained by fitting

$$\sigma_m^{(\mathrm{fit})}(E) = F_m^{(1s)} \sigma_{1s}^{(\mathrm{SD})}(E) + F_m^{(1s+2p)} \sigma_{1s+2p}^{(\mathrm{DD})}(E) + F_m^{(1s+2s)} \sigma_{1s+2s}^{(\mathrm{DD})}(E) \qquad (3)$$

simultaneously to the three experimental cross sections σ_m shown in Fig. 1. The energy-independent factor $F_m^{(1s)}$ adjusts the relative contribution of the $1s$ SD cross section $\sigma_{1s}^{(\mathrm{SD})}(E)$ as appropriate for each σ_m. The factors $F_m^{(1s+2p)}$ and $F_m^{(1s+2s)}$ have the same role for the $1s+2p$ and $1s+2s$ DD processes, respectively. However, the fit does not allow one to disentangle these weight factors from the corresponding DD cross sections. Therefore, Table V, which tabulates the fit results, provides parameters for the *apparent* DD cross sections $\tilde{\sigma}_m^{(DD)}(E) = F_m \sigma^{(DD)}(E)$ with their cross-section maxima $\tilde{\sigma}_m^{(\max)} = F_m \sigma^{(\max)}$ being specific for each m-fold detachment channel [cf. Eq. (1)].

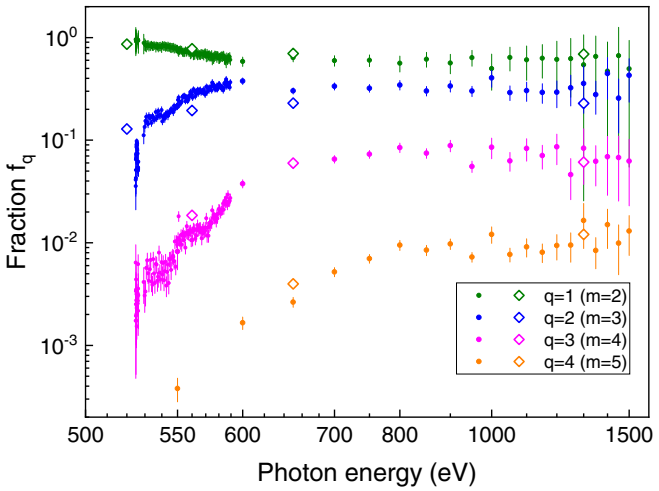

FIG. 2. Experimental (full circles) and theoretical (open diamonds) product-ion charge fractions f_q [Eq. (4)]. The photon-energy (E_{ph}) axis is compressed toward higher energies using $x = \log_{10}(E_{\mathrm{ph}}/\mathrm{eV} - 400)$ for the abscissa.

The $1s{+}2p$ DD and $1s{+}2s$ DD threshold energies that result from the fit (Table V) have a combined fit and systematic uncertainty of less than 1 eV. Within this uncertainty, they agree with the theoretical predictions (Table I). All cross-section maxima decrease when going from triple to fourfold detachment. For $1s$ SD, $1s{+}2p$ DD, and $1s{+}2s$ DD, they are reduced by factors of 0.031, 0.056, and 0.43, respectively; i.e., the relative importance of $1s{+}2s$ DD is higher for fourfold than for triple detachment. For triple detachment, the cross-section maximum of $1s{+}2p$ DD is twice as large as the one of $1s{+}2s$ DD, while for fourfold detachment the latter is nearly a factor of 4 larger than the former. The higher relative yield of O^{3+} ions from the $1s{+}2s$ DD process as compared to $1s{+}2p$ DD can be understood already qualitatively by comparing the respective cascade trees in Tables IV and III. In particular, the chain of the autoionizing transitions $O^+(1s^1\,2s^1\,2p^5) \rightarrow O^{2+}(1s^1\,2s^2\,2p^3) \rightarrow O^{3+}(1s^2\,2s^2\,2p^1)$, which starts with a fast super-Coster-Kronig process, is characteristic for $1s{+}2s$ DD (Table IV).

Our fine-structure-resolved cascade computations, which in addition to single-step autoionizing transitions also consider competing radiative transitions, can be compared quantitatively with the experimental findings. Figure 2 compares experimental and theoretical product-ion charge fractions

$$f_q = \frac{\sigma_{q+1}}{\sigma_\Sigma}, \qquad (4)$$

[1]Parameters for representing the O^- $1s$ SD cross section according to Eqs. (1) and (2) of Ref. [32]: $E_{\mathrm{th}} = 529.6$ eV, $l = 0$, $E_0 = 188.525$ eV, $\sigma_0 = 16.05$ kb, $y_a = 400$, $P = -0.71946$, $y_w = 94.7123$.

TABLE V. Parameter values for expressing the apparent DD cross sections $\tilde{\sigma}_m^{(DD)} = F_m\sigma^{(DD)}(E)$ with $\tilde{\sigma}_m^{(\max)} = F_m\sigma^{(\max)}$ via Eq. (2) with $\alpha = 1.1269$ resulting from the fits discussed in the text. The specific contributions of the $1s$ SD cross section to σ_2, σ_3, and σ_4 are $F_2^{(1s)} = 0.8223(47)$, $F_3^{(1s)} = 0.1723(26)$, and $F_4^{(1s)} = 0.00540(22)$. Numbers in parentheses denote one-σ uncertainties obtained from the fit. The values for $1s$+$1s$ DD bear additional unknown uncertainties associated with "background" subtraction (see text).

Process	$E^{(\mathrm{th})}$ (eV)	$E^{(\max)}$ (eV)	$\tilde{\sigma}_3^{(\max)}$ (kb)	$\tilde{\sigma}_4^{(\max)}$ (kb)	$\tilde{\sigma}_5^{(\max)}$ (kb)
$1s$+$2p$ DD	543.92(29)	575.0(10)	58.4(13)	3.25(14)	
$1s$+$2s$ DD	572.51(59)	680.3(26)	28.1(38)	12.2(02)	
$1s$+$1s$ DD	1010(46)	1627(324)			0.081(17)

where $q = m - 1$ is the product-ion charge state resulting from net m-fold detachment and

$$\sigma_\Sigma = \sum_{m=2}^{5} \sigma_m = \sum_{q=1}^{4} \sigma_{q+1}. \tag{5}$$

Theoretical f_q values have been computed for the photon energies 520, 560, 650, and 1300 eV (Fig. 2), which are above the thresholds for $1s$ SD, $1s$+$2p$ DD, $1s$+$2s$ DD, and $1s$+$1s$ DD, respectively. In these computations, the F_m values which result from our cascade calculations and which are provided in Table VI have been weighted with the relative cross sections for the individual SD and DD processes as discussed in the following.

At 520 eV, a $1s$ hole can be created only via $1s$ SD. Accordingly, $f_q(520\,\mathrm{eV}) = F_m^{(1s)}$. The subsequent single-step cascade tree produces O^{2+} as the highest charged product ion (Table II). The theoretical O^+ and O^{2+} fractions of 86% and 13% (Table VI) agree well with the corresponding experimental $F_m^{(1s)}$ values (caption of Table V). A fraction of 1% is theoretically predicted for neutral oxygen, which cannot be observed in the present experimental configuration. The small experimentally observed O^{3+} fraction can only be explained if higher order processes are taken into account such as multiple Auger processes (see, e.g., Refs. [25,36]). Such processes were, however, not considered in the present cascade calculations.

At 560 eV, the $1s$+$2p$ DD process is energetically allowed in addition to $1s$ SD. Now the maximum calculated charge state that can be reached by single-step de-excitation cascades, is 3+ (Table III). In the absence of a rigorous theoretical treatment of direct double-detachment processes, we just assumed in our calculations that the $1s$+$2p$ DD process contributes by 10% to the total detachment cross section, which is of the same order of magnitude as the shake probabilities mentioned in Sec. III. Accordingly, $f_q(560\,\mathrm{eV}) = 0.9F_m^{(1s)} + 0.1F_m^{(1s+2p)}$. The resulting fractions of net double, triple, and fourfold detachment agree surprisingly well with the experimental findings considering the coarseness of this approach. The same holds at 650 eV, which is above the threshold for $1s$+$2s$ DD and where our cascade calculations also predict a nonzero contribution by net fivefold detachment. In analogy to the $1s$+$2p$ DD process, $1s$+$2s$ DD also received a weight of 10% such that $f_q(650\,\mathrm{eV}) = 0.8F_m^{(1s)} + 0.1F_m^{(1s+2p)} + 0.1F_m^{(1s+2s)}$. At 1300 eV, i.e., above the threshold for $1s$+$1s$ DD, a 1% contribution from this latter process has been assumed in addition and, correspondingly, $f_q(1300\,\mathrm{eV}) = 0.79F_m^{(1s)} + 0.1F_m^{(1s+2p)} + 0.1F_m^{(1s+2s)} + 0.01F_m^{(1s+1s)}$.

In our measurements, we scrutinized the weak O^{4+} product-ion channel in the search for a signature of double K-hole formation via the $1s$+$1s$ DD process. According to our calculations, the threshold for direct double K-shell detachment occurs at 1160 eV (Table I). Around this energy, the cross section σ_5 exhibits a noticeable rise which is not present in σ_3 and σ_4 (Fig. 3). These latter two cross sections show identical high-energy behaviors, which can be described by

TABLE VI. Theoretical product-ion charge-state distributions resulting from the present cascade calculations for $1s$ SD ($F_m^{(1s)}$), $1s$+$2p$ DD ($F_m^{(1s+2p)}$), $1s$+$2s$ DD ($F_m^{(1s+2s)}$), and $1s$+$1s$ DD ($F_m^{(1s+1s)}$). The quantity q denotes the product-ion charge state which equals $m - 1$ [Eq. (1)].

q	m	$F_m^{(1s)}$	$F_m^{(1s+2p)}$	$F_m^{(1s+2s)}$	$F_m^{(1s+1s)}$
0	1	0.011	0.0	0.0	0.0
1	2	0.861	0.029	0.069	0.001
2	3	0.128	0.786	0.478	0.069
3	4	0.0	0.185	0.413	0.120
4	5	0.0	0.0	0.040	0.810
5	6	0.0	0.0	0.0	0.0

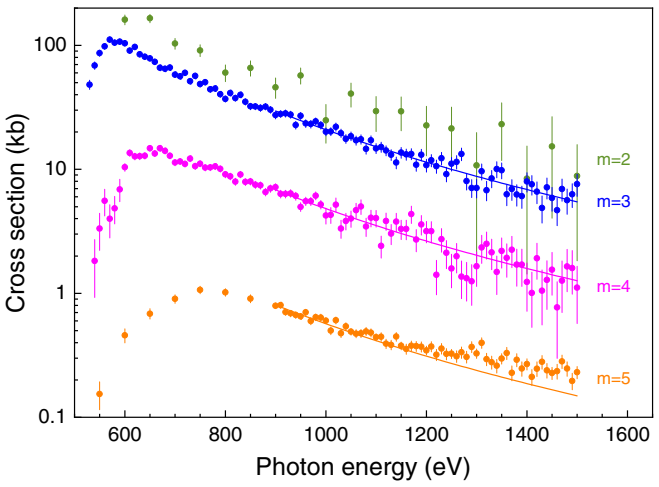

FIG. 3. Results from coarse photon-energy scans over a wide range. The differently colored data points represent the experimental cross sections σ_m for multiple [m-fold, Eq. (1)] detachment of O^- ions for m=2 (olive), m=3 (blue), m=4 (magenta), and m=5 (orange). The error bars account only for the statistical experimental uncertainties. The full lines represent a power law with the exponent -3.3 ± 0.1 as obtained from a fit to σ_3 (see text).

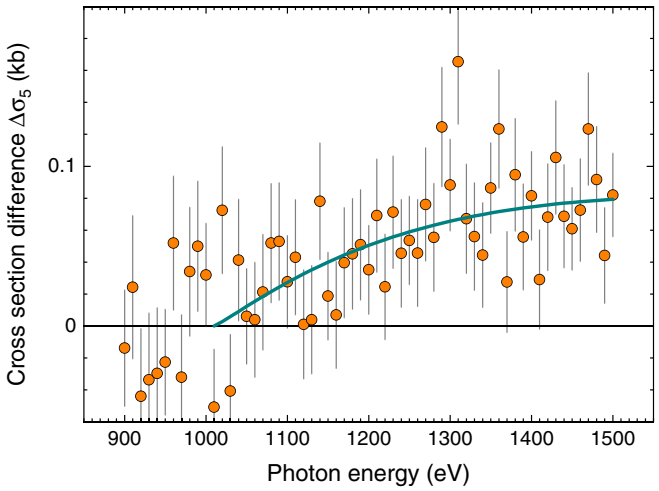

FIG. 4. Cross-section difference resulting from the subtraction of the scaled power-law fit from the measured cross section σ_5 (see Fig. 3). The full line results from a fit of the Pattard formula [Eq. (2)] to the data points. The fit results are listed in Table V.

a power law with an exponent of -3.3. This number was obtained from a fit to σ_3, and the resulting fit curve was then scaled to σ_4 and σ_5 by multiplication with appropriate factors (full lines in Fig. 3).

The data points in Fig. 4 were obtained by subtracting the appropriately scaled power law from the measured cross section σ_5. This cross-section difference $\Delta\sigma_5$ is zero up to about 1000 eV from where about it rises toward higher energies. A fit of Eq. (2) to the data points yields a threshold value of 1010 ± 46 eV (Table V) which is somewhat lower than our calculated value. Conceding an additional (unknown) uncertainty related to the subtraction of the power-law curve, it seems nevertheless plausible that the cross-section difference depicted in Fig. 4 is indeed due to $1s{+}1s$ DD.

The fit of the Pattard formula [Eq. (2)] yields a maximum value of the $1s{+}1s$ DD cross section of 81 ± 17 b. This is significantly smaller than the maximum cross section of 3 kb which we have found earlier for fivefold detachment of C^- [7]. This can be (at least partly) attributed to the general strong decrease of double-photoionization cross sections with increasing nuclear charge [37]. Moreover, it cannot be excluded that $1s{+}1s$ DD also contributes to the production of final ion charge states other than O^{4+}. Our cascade calculations result in a product charge-state distribution that consists of 7% O^{2+}, 12% O^{3+}, 81% O^{4+}, and 0% O^{5+} ions ($F_m^{(1s+1s)}$ in Table VI). At the present level of statistical uncertainty, a $\approx$10% contribution of $1s{+}1s$ DD to σ_4 can remain unnoticed considering the scatter of the experimental σ_4 data points above 1000 eV (Fig. 3). We also scrutinized the O^{5+} channel, but the count rate was too low for a measurement of σ_6 with satisfying statistical uncertainty in a reasonable amount of time.

It should be noted that the measurement of the small cross section σ_5, which is in the sub-kilobarn range, is particularly challenging. In addition, at photon energies above 1000 eV, the photon flux at the PETRA III photon beamline P04 decreases rapidly as the photon energy increases, so that it becomes difficult to measure small cross sections with sufficient statistical accuracy when going to higher energies. In the present experiment, the lowest O^{4+} count rate was only 0.2 Hz. Nevertheless, this is still an order of magnitude larger than the dark-count rate ($\approx$0.02 Hz, see Sec. II) of our single-particle detector. This rules out that the rise of σ_5 beyond $\approx$1100 eV is an artifact of our product-ion detection scheme. In this context, we mention our recent measurement of the similarly small cross section for sixfold photoionization of Ar^+ ions [25].

V. SUMMARY AND CONCLUSIONS

Employing the photon-ion merged-beams technique at a high-flux beamline of one of the world's brightest synchrotron-radiation facilities, we were able to measure cross sections for the single-photon multiple inner-shell photodetachment of oxygen anions over a wide energy range extending to well beyond the threshold for double K-shell detachment. Owing to a high product-ion selectivity and a near 100% product-ion detection efficiency, we were able to measure cross sections for net double, triple, fourfold, and fivefold ionization. These turned out to be dominated by direct double-detachment processes where one photon simultaneously ejects two electrons. As in our previous studies on F^- [6] and C^- [7], the experimental cross-section shapes are very well described by the empirical scaling formula suggested by Pattard [34]. In future experiments, more detailed information might be obtained from electron spectroscopy. Although this is rather demanding, mainly because of the low densities of ionic targets, first steps in this direction have already been taken [38–40].

We identified the various single and double detachment thresholds by large-scale atomic-structure calculations which also account for the complex deexcitation cascades that set in after the initial core-hole creation. The theoretical results for the product charge-state distributions agree well with the experimental findings despite of the fact that only single Auger and radiative dipole transitions were considered in the computation of the de-excitation cascades. The calculations do not predict any yield of O^{4+} product ions below the threshold for $1s{+}1s$ double ionization although a small experimental cross for fivefold detachment could be measured. This suggests that many-electron processes such as detachment accompanied by shake-up or double-Auger processes are decisive for the production of O^{4+} ions. In the future, we will incorporate such processes into our systematic approach for the computation of de-excitation cascades [17]. Even more theoretical development work is required for a more quantitative understanding of the various double-ionization processes at play.

ACKNOWLEDGMENTS

We acknowledge DESY (Hamburg, Germany), a member of the Helmholtz Association HGF, for the provision of experimental facilities. Parts of this research were carried out at PETRA III and we would like to thank Kai Bagschik, Frank Scholz, Jörn Seltmann, and Moritz Hoesch for assistance in using beamline P04. We are grateful for support from

Bundesministerium für Bildung und Forschung within the "Verbundforschung" funding scheme (Grants No. 05K19GU3 and No. 05K19RG3) and from Deutsche Forschungsgemeinschaft (DFG, Projects No. 389115454 and No. SFB925/A3).

[1] H. Hotop and W. C. Lineberger, Binding energies in atomic negative ions, J. Phys. Chem. Ref. Data **4**, 539 (1975).

[2] D. J. Pegg, Structure and dynamics of negative ions, Rep. Prog. Phys. **67**, 857 (2004).

[3] T. Andersen, Atomic negative ions: Structure, dynamics, and collisions, Phys. Rep. **394**, 157 (2004).

[4] C. Blondel, C. Delsart, C. Valli, S. Yiou, M. R. Godefroid, and S. Van Eck, Electron affinities of ^{16}O,^{17}O, ^{18}O, the fine structure of $^{16}O^-$ and the hyperfine structure of $^{17}O^-$, Phys. Rev. A **64**, 052504 (2001).

[5] A. Kramida, Y. Ralchenko, J. Reader, and NIST ASD Team, NIST Atomic Spectra Database, version 5.9, Tech. Rep., National Institute of Standards and Technology, 2021, http://physics.nist.gov/asd.

[6] A. Müller, A. Borovik Jr., S. Bari, T. Buhr, K. Holste, M. Martins, A. Perry-Saßmannshausen, R. A. Phaneuf, S. Reinwardt, S. Ricz, K. Schubert, and S. Schippers, Near-K-Edge Double and Triple Detachment of the F^- Negative Ion: Observation of Direct Two-Electron Ejection by a Single Photon, Phys. Rev. Lett. **120**, 133202 (2018).

[7] A. Perry-Sassmannshausen, T. Buhr, A. Borovik Jr., M. Martins, S. Reinwardt, S. Ricz, S. O. Stock, F. Trinter, A. Müller, S. Fritzsche, and S. Schippers, Multiple Photodetachment of Carbon Anions Via Single and Double Core-Hole Creation, Phys. Rev. Lett. **124**, 083203 (2020).

[8] S. Schippers, A. Perry-Sassmannshausen, T. Buhr, M. Martins, S. Fritzsche, and A. Müller, Multiple photodetachment of atomic anions via single and double core-hole creation, J. Phys. B: At. Mol. Opt. Phys. **53**, 192001 (2020).

[9] A. S. Kheifets, Dynamic scaling of photo-double-ionization to electron impact, Phys. Rev. A **101**, 032701 (2020).

[10] P. Lablanquie, F. Penent, and Y. Hikosaka, Multi-electron coincidence spectroscopy: Double photoionization from molecular inner-shell orbitals, J. Phys. B: At. Mol. Opt. Phys. **49**, 182002 (2016).

[11] J. B. Donahue, P. A. M. Gram, M. V. Hynes, R. W. Hamm, C. A. Frost, H. C. Bryant, K. B. Butterfield, D. A. Clark, and W. W. Smith, Observation of Two-Electron Photoionization of the H^- Ion Near Threshold, Phys. Rev. Lett. **48**, 1538 (1982).

[12] Y. K. Bae, M. J. Coggiola, and J. R. Peterson, Absolute cross section for near-threshold two-electron photoionization of He^-, Phys. Rev. A **28**, 3378 (1983).

[13] Y. K. Bae and J. R. Peterson, Near-threshold measurements of K^- two-electron photoionization cross sections, Phys. Rev. A **37**, 3254 (1988).

[14] N. D. Gibson, R. C. Bilodeau, C. W. Walter, D. Hanstorp, A. Aguilar, N. Berrah, D. J. Matyas, Y.-G. Li, R. M. Alton, and S. E. Lou, K-shell photodetachment from O^-, J. Phys.: Conf. Ser. **388**, 022102 (2012).

[15] S. Schippers, R. Beerwerth, L. Abrok, S. Bari, T. Buhr, M. Martins, S. Ricz, J. Viefhaus, S. Fritzsche, and A. Müller, Prominent role of multielectron processes in K-shell double and triple photodetachment of oxygen anions, Phys. Rev. A **94**, 041401(R) (2016).

[16] S. Fritzsche, A fresh computational approach to atomic structures, processes, and cascades, Comput. Phys. Commun. **240**, 1 (2019).

[17] S. Fritzsche, P. Palmeri, and S. Schippers, Atomic cascade computations, Symmetry **13**, 520 (2021).

[18] S. Schippers, A. L. D. Kilcoyne, R. A. Phaneuf, and A. Müller, Photoionisation of ions with synchrotron radiation: From ions in space to atoms in cages, Contemp. Phys. **57**, 215 (2016).

[19] S. Schippers, S. Ricz, T. Buhr, A. Borovik Jr., J. Hellhund, K. Holste, K. Huber, H.-J. Schäfer, D. Schury, S. Klumpp, K. Mertens, M. Martins, R. Flesch, G. Ulrich, E. Rühl, T. Jahnke, J. Lower, D. Metz, L. P. H. Schmidt, M. Schöffler *et al.*, Absolute cross sections for photoionization of Xe^{q+} ions ($1 \leqslant q \leqslant 5$) at the 3d ionization threshold, J. Phys. B **47**, 115602 (2014).

[20] A. Müller, D. Bernhardt, A. Borovik Jr., T. Buhr, J. Hellhund, K. Holste, A. L. D. Kilcoyne, S. Klumpp, M. Martins, S. Ricz, J. Seltmann, J. Viefhaus, and S. Schippers, Photoionization of Ne atoms and Ne^+ ions near the K edge: Precision spectroscopy and absolute cross-sections, Astrophys. J. **836**, 166 (2017).

[21] S. Schippers, T. Buhr, A. Borovik Jr., K. Holste, A. Perry-Sassmannshausen, K. Mertens, S. Reinwardt, M. Martins, S. Klumpp, K. Schubert, S. Bari, R. Beerwerth, S. Fritzsche, S. Ricz, J. Hellhund, and A. Müller, The photon-ion merged-beams experiment PIPE at PETRA III - The first five years, X-Ray Spectrom. **49**, 11 (2020).

[22] J. Viefhaus, F. Scholz, S. Deinert, L. Glaser, M. Ilchen, J. Seltmann, P. Walter, and F. Siewert, The variable polarization XUV beamline P04 at PETRA III: Optics, mechanics, and their performance, Nucl. Instrum. Methods Phys. Res., Sect. A **710**, 151 (2013).

[23] R. Middleton, A versatile high intensity negative ion source, Nucl. Instrum. Methods **220**, 105 (1984).

[24] K. Rinn, A. Müller, H. Eichenauer, and E. Salzborn, Development of single-particle detectors for keV ions, Rev. Sci. Instrum. **53**, 829 (1982).

[25] A. Müller, M. Martins, A. Borovik Jr., T. Buhr, A. Perry-Sassmannshausen, S. Reinwardt, F. Trinter, S. Schippers, S. Fritzsche, and A. S. Kheifets, Role of *L*-shell single and double core-hole production and decay in *m*-fold ($1 \leqslant m \leqslant 6$) photoionization of the Ar^+ ion, Phys. Rev. A **104**, 033105 (2021).

[26] A. Müller, E. Lindroth, S. Bari, A. Borovik Jr., P.-M. Hillenbrand, K. Holste, P. Indelicato, A. L. D. Kilcoyne, S. Klumpp, M. Martins, J. Viefhaus, P. Wilhelm, and S. Schippers, Photoionization of metastable heliumlike $C^{4+}(1s\,2s\,{}^3S_1)$ ions: Precision study of intermediate doubly excited states, Phys. Rev. A **98**, 033416 (2018).

[27] I. P. Grant, *Relativistic Quantum Theory of Atoms and Molecules: Theory and Computation* (Springer, New York, 2007).

[28] S. Fritzsche, Large-scale accurate structure calculations for open-shell atoms and ions, Phys. Scr. **T100**, 37 (2002).

[29] S. Fritzsche, JAC: User guide, compendium, and theoretical background [https://github.com/OpenJAC/JAC.jl].

[30] A. Perry-Sassmannshausen, T. Buhr, M. Martins, S. Reinwardt, F. Trinter, A. Müller, S. Fritzsche, and S. Schippers, Multiple photodetachment of silicon anions via K-shell excitation and ionization, Phys. Rev. A **104**, 053107 (2021).

[31] S. Fritzsche, B. Fricke, and W.-D. Sepp, Reduced L_1 level width and Coster-Kronig yields by relaxation and continuum interactions in atomic zinc, Phys. Rev. A **45**, 1465 (1992).

[32] D. A. Verner, D. G. Yakovlev, I. M. Band, and M. B. Trzhaskovskaya, Subshell photoionization cross sections and ionization energies of atoms and ions from He to Zn, At. Data Nucl. Data Tables **55**, 233 (1993).

[33] A. Müller, A. L. D. Kilcoyne, R. A. Phaneuf, K. Holste, S. Schippers, and A. S. Kheifets, Direct double ionization of the Ar^+ M shell by a single photon, Phys. Rev. A **103**, L031101 (2021).

[34] T. Pattard, A shape function for single-photon multiple ionization cross sections, J. Phys. B: At. Mol. Opt. Phys. **35**, L207 (2002).

[35] G. H. Wannier, The threshold law for single ionization of atoms or ions by electrons, Phys. Rev. **90**, 817 (1953).

[36] A. Müller, A. Borovik Jr., T. Buhr, J. Hellhund, K. Holste, A. L. D. Kilcoyne, S. Klumpp, M. Martins, S. Ricz, J. Viefhaus, and S. Schippers, Observation of a Four-Electron Auger Process in Near-K-Edge Photoionization of Singly Charged Carbon Ions, Phys. Rev. Lett. **114**, 013002 (2015).

[37] J. Hoszowska, A. K. Kheifets, J.-C. Dousse, M. Berset, I. Bray, W. Cao, K. Fennane, Y. Kayser, M. Kavčič, J. Szlachetko, and M. Szlachetko, Physical Mechanisms and Scaling Laws of K-Shell Double Photoionization, Phys. Rev. Lett. **102**, 073006 (2009).

[38] C. Domesle, B. Jordon-Thaden, L. Lammich, M. Förstel, U. Hergenhahn, A. Wolf, and H. B. Pedersen, Photoelectron spectroscopy of O^- at 266 nm: Ratio of ground- and excited-state atomic oxygen production and channel-resolved photoelectron anisotropy parameters, Phys. Rev. A **82**, 033402 (2010).

[39] L. S. Harbo, A. Becker, S. Dziarzhytski, C. Domesle, N. Guerassimova, A. Wolf, and H. B. Pedersen, Single and double electron photodetachment from the oxygen anion at 41.7 nm, Phys. Rev. A **86**, 023409 (2012).

[40] J.-M. Bizau, D. Cubaynes, S. Guilbaud, F. Penent, P. Lablanquie, L. Andric, J. Palaudoux, M. M. Al Shorman, and C. Blancard, Photoelectron Spectroscopy of Ions: Study of the Auger Decay of the $4d \rightarrow nf$ $(n = 4, 5)$ Resonances in Xe^{5+} Ion, Phys. Rev. Lett. **116**, 103001 (2016).